Biogeosciences Discuss., 12, 13967–14002, 2015
www.biogeosciences-discuss.net/12/13967/2015/
doi:10.5194/bgd-12-13967-2015

Biogeosciences Discussions
Open Access

Uncertainty analysis of gross primary production partitioned from net ecosystem exchange measurements

R. Raj, N. A. S. Hamm, C. van der Tol, and A. Stein

Faculty of Geo-Information Science and Earth Observation (ITC), University of Twente, PO Box 217, 7514 AE Enschede, the Netherlands

Received: 8 July 2015 – Accepted: 6 August 2015 – Published: 26 August 2015

Correspondence to: R. Raj (r.raj@utwente.nl)

Published by Copernicus Publications on behalf of the European Geosciences Union.

Abstract

Gross primary production (GPP), separated from flux tower measurements of net ecosystem exchange (NEE) of CO_2, is used increasingly to validate process-based simulators and remote sensing-derived estimates of simulated GPP at various time steps. Proper validation should include the uncertainty associated with this separation at different time steps. This can be achieved by using a Bayesian framework. In this study, we estimated the uncertainty in GPP at half hourly time steps. We used a non-rectangular hyperbola (NRH) model to separate GPP from flux tower measurements of NEE at the Speulderbos forest site, The Netherlands. The NRH model included the variables that influence GPP, in particular radiation, and temperature. In addition, the NRH model provided a robust empirical relationship between radiation and GPP by including the degree of curvature of the light response curve. Parameters of the NRH model were fitted to the measured NEE data for every 10-day period during the growing season (April to October) in 2009. Adopting a Bayesian approach, we defined the prior distribution of each NRH parameter. Markov chain Monte Carlo (MCMC) simulation was used to update the prior distribution of each NRH parameter. This allowed us to estimate the uncertainty in the separated GPP at half-hourly time steps. This yielded the posterior distribution of GPP at each half hour and allowed the quantification of uncertainty. The time series of posterior distributions thus obtained allowed us to estimate the uncertainty at daily time steps. We compared the informative with non-informative prior distributions of the NRH parameters. The results showed that both choices of prior produced similar posterior distributions GPP. This will provide relevant and important information for the validation of process-based simulators in the future. Furthermore, the obtained posterior distributions of NEE and the NRH parameters are of interest for a range of applications.

BGD
12, 13967–14002, 2015

1 Introduction

Net ecosystem exchange (NEE) is a terrestrial component of the global carbon cycle. It is the exchange of CO_2 between the terrestrial ecosystem and the atmosphere. The measurement of NEE by the eddy covariance technique is well-established (Baldocchi, 2003). Specifically, NEE is the balance between the CO_2 released by the ecosystem respiration (R_{eco}) and the gross CO_2 assimilated via photosynthesis. The fraction of carbon in the assimilated CO_2 is the gross primary production (GPP). Estimates of GPP, which is partitioned from NEE, provides information about the physiological processes that contribute to NEE (Aubinet et al., 2012). Measured NEE data are used to validate the NEE that is simulated by ecosystem process-based simulators such as BIOME-BGC (BioGeochemical Cycles) (Thornton, 1998). It is often desirable to validate the simulated component flux independently. This is particularly important for diagnosing the misrepresentation (overestimation or underestimation) of assimilation processes in the simulator (Reichstein et al., 2005), which can only be achieved by comparing the GPP partitioned from NEE data with the simulated one. Furthermore, remote sensing derived light use efficiency (LUE) models address the spatial and temporal dynamics of GPP (Running et al., 2004). The reliability of such models at the regional scale relies on the validation using GPP partitioned from NEE data (Wang et al., 2010; Li et al., 2013).

Flux partitioning methods (FPM) are used to partition NEE into its component flux (GPP and R_{eco}). These methods are based on fitting a non-linear empirical models to the measured NEE data and other meteorological data in order to estimate the parameters. The estimated parameters of the non-linear model then used to predict daytime R_{eco} and GPP. There are two types of FPM: (1) those that use only nighttime NEE data (2) those that use either daytime NEE data or both daytime and nighttime data (Lasslop et al., 2010; Stoy et al., 2006; Aubinet et al., 2012).

A nighttime-based FPM assumes that NEE is equal to R_{eco} (GPP = 0 during the night) and that it varies with air and soil temperature (Richardson et al., 2006).

BGD
12, 13967–14002, 2015

A daytime-based FPM assumes that the variation of NEE occurs with photosynthetic photon flux density (PPFD) and the light response curve (plot of NEE against PPFD) can be represented by a rectangular hyperbola (RH) model (Ruimy et al., 1995). Gilmanov et al. (2003) proposed a daytime-based FPM that uses the non-rectangular hyperbola (NRH) model to incorporate the effect of the degree of curvature (θ) of the light response curve (i.e., the convexity of the light response curve as the NEE and radiation relationship approaches saturation). Further, the light response curve represented by the NRH model has been found to fit NEE data better than the RH model (Gilmanov et al., 2003; Aubinet et al., 2012). Lasslop et al. (2010) proposed a daytime-based FPM using the RH model by incorporating the variation of NEE as a function of global radiation, air temperature, and vapor pressure deficit (VPD) because these affect GPP via stomatal regulation. Recently, Gilmanov et al. (2013) modified the NRH model by incorporating the effect of VPD and temperature as proposed by Lasslop et al. (2010). They used PPFD and soil temperature instead of global radiation and air temperature respectively. This modification incorporates the influence of PPFD, air or soil temperature, VPD, and θ by taking advantage of better representation of the light response curve by comparison to the RH model.

A quantification of uncertainty in partitioned GPP provides an associated credible interval that can be used for proper implementation of calibration and validation of a process-based simulator against partitioned GPP (Hagen et al., 2006). The temporal resolution of process-based simulators may vary from half-hourly to monthly. It is therefore necessary to quantify uncertainty associated with the partitioned GPP at half-hourly to monthly time scales. For example, the partitioned GPP and associated uncertainty at a daily time scale can provide data for the calibration of BIOME-BGC.

In this study, we adopted the NRH model to partition half-hourly GPP from NEE data. Previously numerical optimization has been used to estimate a single optimized values of the model parameters (Gilmanov et al., 2003, 2013). This did not quantify the uncertainty in half-hourly partitioned GPP. The measurements of half-hourly NEE are uncertain. Therefore, the optimized parameters are also uncertain (Richardson and

BGD
12, 13967–14002, 2015

Hollinger, 2005). Obtaining the underlying probability distribution of the NRH parameters gives a measure of uncertainty in parameters, which can be further propagated towards the NRH model to estimate uncertainty in partitioned GPP. A Bayesian implementation provides a solution to quantify the uncertainty in model parameters in the form of probability distributions (Gelman et al., 2013). The Bayesian approach was used in other studies to constrain the parameters of process-based simulators by using either eddy covariance data, biometric data, or both (Du et al., 2015; Minet et al., 2015; Ricciuto et al., 2008). We applied the Bayesian approach to a different type of model. We fitted the non-linear empirical NRH model to NEE data and quantified the uncertainty in NRH parameters to partition GPP with uncertainty.

The objective of this study was to implement a Bayesian approach to quantify the uncertainty in half-hourly partitioned GPP using the NRH model given the availability of half-hourly NEE and other meteorological data. The time series of empirical distributions of half-hourly GPP values also allowed us to estimate the uncertainty in GPP at daily time steps. Data were available from a flux tower in the central Netherlands at the Speulderbos forest. This will provide relevant and important information for the validation of process-based simulators.

2 Methods

2.1 The non-rectangular hyperbola (NRH) model

NEE is given as:

$$\mathrm{NEE} = P_a - R_{eco} \quad (1)$$

where NEE is measured by the eddy covariance technique and P_a is gross CO_2 assimilation. We adopted the sign convention used by ecosystem scientists in which the exchange of carbon into the system through photosynthesis is considered a positive flux and loss of carbon through respiration is considered a negative flux.

BGD
12, 13967–14002, 2015

The light response curve is represented using the NRH model (Gilmanov et al., 2003):

$$P_a = \frac{1}{2\theta} \times \left(\alpha \cdot \mathrm{PPFD} + A_{max} - \sqrt{(\alpha \cdot \mathrm{PPFD} + A_{max})^2 - 4\alpha \cdot A_{max} \cdot \theta \cdot \mathrm{PPFD}}\right) \quad (2)$$

where α is the apparent quantum yield, A_{max} is the photosynthetic capacity at light saturation, and θ is the degree of curvature of the light response curve.

Gilmanov et al. (2013) modelled ecosystem respiration R_{eco} using the air temperature T_a as a dominant driver according to Van't-Hoff's equation in its exponential form (Thornley and Johnson, 2000):

$$R_{eco} = r_0 \times \exp(k_T T_a) \quad (3)$$

where r_0 and k_T are the temperature sensitivity coefficients. Eqs. 2 and 3 are substituted in Eq. (1) to obtain the model for net ecosystem exchange NEE:

$$\mathrm{NEE} = \frac{1}{2\theta} \times \left(\alpha \cdot \mathrm{PPFD} + A_{max} - \sqrt{(\alpha \cdot \mathrm{PPFD} + A_{max})^2 - 4\alpha \cdot A_{max} \cdot \theta \cdot \mathrm{PPFD}}\right) - r_0 \times \exp(k_T T_a). \quad (4)$$

Both daytime and nighttime half-hourly NEE, PPFD, and T_a data were used to estimate the NRH model parameters $\boldsymbol{\beta} = (\theta, \alpha, A_{max}, r_0, k_T)$ (Eq. 4). For nighttime data, Eq. (4) includes only the respiration term as PPFD is equal to zero during the night. These estimated parameters, together with half-hourly PPFD, were used in Eq. (2) to calculate half-hourly P_a. Values of half-hourly GPP were calculated by multiplying P_a by 12/44 (12 is the atomic mass of carbon, and 44 is the atomic mass of CO_2). The unit of each parameter and other variables used in the above equations are shown in Table 1.

BGD
12, 13967–14002, 2015

2.2 Bayesian inference for model parameters

Bayesian inference treats all parameters as random variables (Gelman et al., 2013). Bayes rule is given as

$$p(\boldsymbol{\beta}|\mathbf{y}) = \frac{p(\mathbf{y}|\boldsymbol{\beta})p(\boldsymbol{\beta})}{p(\mathbf{y})} \propto \text{likelihood} \times \text{prior} \quad (5)$$

where $p(\boldsymbol{\beta})$ is the prior distribution, representing the prior understanding of uncertainty in the model parameters values before the observations are taken into account. This understanding may come from expert judgement or previously published research on the parameters (Oakley and O'Hagan, 2007; Raj et al., 2014). If no prior knowledge is available non-informative priors may be used (i.e., a wide prior distribution that conveys no prior information). The term $p(\boldsymbol{\beta}|\mathbf{y})$ is the posterior distribution of $\boldsymbol{\beta}$ after combining prior knowledge and data $\mathbf{y}$ and represents the uncertainty in $\boldsymbol{\beta}$ given the data and the prior. The marginal effect of each parameter $p(\beta_i|\mathbf{y}), i = 1, 2, \ldots, n$, is the main quantity of interest, expressing the uncertainty in each parameter separately. The term $p(\mathbf{y}|\boldsymbol{\beta})$ is the conditional probability of observing data $\mathbf{y}$ given $\boldsymbol{\beta}$ and is also called the likelihood. The term $p(\mathbf{y})$ is the probability of observing the data $\mathbf{y}$ before observations were taken. This acts as the normalising constant that ensures that $p(\boldsymbol{\beta}|\mathbf{y})$ is a valid probability distribution that integrates to 1. For most real-world problems it is not possible to write down analytical solutions for Eq. (5) and it is usual to perform inference using Markov Chain Monte Carlo (MCMC) simulation (Gelman et al., 2013).

MCMC is a method for conducting inference on $p(\boldsymbol{\beta}|\mathbf{y})$. It requires evaluation of the joint distribution $p(\mathbf{y}|\boldsymbol{\beta})p(\boldsymbol{\beta})$, which represents the dependence structure in the data. MCMC constructs Markov chains of the parameters space and generates samples $\boldsymbol{\beta}^{(1)}, \boldsymbol{\beta}^{(2)}, \ldots, \boldsymbol{\beta}^{(m)}$ of $\boldsymbol{\beta}$ whose unique stationary distribution is the posterior distribution of interest $p(\boldsymbol{\beta}|\mathbf{y})$. The m samples are then used to conduct inference on each β_i. For example the mean, median and 95 % credible interval can all be calculated over these m samples. It is usual to construct multiple Markov chains and to assess whether they converge to the same stationary distribution.

BGD
12, 13967–14002, 2015

3 Bayesian inference for the NRH model parameters

3.1 Study area and data

The Speulderbos forest is located at 52°15′08″ N, 5°41′25″ E within a large forested area in the Netherlands. There is a flux tower within a dense 2.5 ha Douglas fir stand. The stand was planted in 1962. The vegetation, soil, and climate of this site have been thoroughly described elsewhere (Steingrover and Jans, 1994; Su et al., 2009; van Wijk et al., 2001).

The CSAT3, Cambell Sci, LI7500 LiCor Inc, and CR5000 instruments were installed in June 2006 and have been maintained, and the data processed (software AltEddy, Alterra) by C. van der Tol (University of Twente, co-author) and A. Frumau (Energy Centre Netherlands). We examined half-hourly NEE data (measured at the flux tower) for the growing season (April to October) of 2009. NEE data were corrected for storage of CO_2 in the air between the sensor and the ground. The quality of NEE data was assessed using the Foken classification system, which provides a flag to each half-hourly NEE datum from 1 through 9 (Foken et al., 2005). Each flag is associated with: (a) the range of the steady state condition of the covariance of vertical wind speed and CO_2 concentration of half-hour duration, (b) the range of the integral turbulence characteristic parameter indicating the developed turbulence; and (c) the range of the orientation of the sonic anemometer to make sure that the probe is omnidirectional at the time of measurements. We followed the suggestion of Foken et al. (2005) and accepted only those NEE data that were labelled from 1 to 3.

Half-hourly PPFD and T_a from the flux tower were used as variables in Eq. (4). Gilmanov et al. (2013) proposed to incorporate the effect of VPD by multiplying Eq. (2) by the VPD-response function, ϕ, that accounts for the VPD limitation on P_a. The function ϕ is set equal to 1 if VPD is below some critical value (VPD_{cr}) that indicates that water stress does not affect photosynthesis. Above the critical value ($VPD > VPD_{cr}$), ϕ decreases exponentially with the curvature parameter σ_{VPD}, which may vary between 1 and 30 kPa. Low values of σ_{VPD} indicate a strong water stress effect, whereas higher

BGD
12, 13967–14002, 2015

values indicate a weak water stress effect. We calculated half-hourly VPD from relative humidity (RH) using the procedure provided in Monteith and Unsworth (1990). We found that 90 % of the total half-hourly VPD values in the growing season of 2009 were less than 1 kPa and 9 % were between 1 kPa and 1.5 kPa. We therefore neglected the influence of VPD as a limiting factor for the water stress at Speulderbos. This follows Körner (1995) and Lasslop et al. (2010) who specified $\mathrm{VPD}_{\mathrm{cr}} = 1$. We, therefore, assumed ϕ equal to 1.

3.2 Bayesian implementation

We treated Eq. (4) as a non-linear regression problem:

$$y_i = \frac{1}{2\theta} \times \left(\alpha \cdot \mathrm{PPFD}_i + A_{\max} - \sqrt{(\alpha \cdot \mathrm{PPFD}_i + A_{\max})^2 - 4\alpha \cdot A_{\max} \cdot \theta \cdot \mathrm{PPFD}_i}\right) - r_0 \times \exp\left(k_{\mathrm{T}} T_{\mathrm{a}_i}\right) + \varepsilon_i = \mu_i - v_i + \varepsilon_i \quad (6)$$

where y is the response variable (NEE), PPFD and T_{a} are predictor variables and ε is the residual error. The residual error arose because the model did not perfectly fit the data. The subscript i indicates a single observation. For brevity we use μ_i to refer to the first term on the RHS and v_i to refer to the second term on the RHS.

As is common in regression, we assumed normally distributed errors, hence $\varepsilon_i \sim N(0, \sigma^2)$ and the likelihood also followed a normal distribution, such that $y_i \sim N(\mu_i - v_i, \sigma^2)$. In the above notation, $\boldsymbol{\beta} = (\alpha, A_{\max}, \theta, r_0, k_{\mathrm{T}})^T$ and the likelihood is $p(\mathbf{y}|\boldsymbol{\beta}, \sigma^2)$, where $\mathbf{y} = (y_1, y_2, \ldots, y_n)^T$ for n observations.

In Bayesian analysis it is usual to refer to precision, which is the inverse of the variance, hence $\tau_e = 1/\sigma^2$. No prior information was available for τ_e so a non-informative prior was selected. A Gamma distribution with shape and rate parameters equal to 0.001 ensures a non-negative non-informative prior for τ_e (Lunn et al., 2013).

BGD
12, 13967–14002, 2015

We made two choices for the prior distribution for each β_i. First, a non-informative prior was used. Second prior information for each β_i was obtained from the literature. Note that the same non-informative prior for τ_e was used in both cases. The results for informative an non-informative priors were compared.

3.2.1 Non-informative prior distributions

We assumed a normal distribution for each β_i with mean equal to 0 and standard deviation equal to 32, which gives small value of the the precision equal to 0.001 to make the distribution wide. NRH is a non-linear model and therefore appropriate constraints should be imposed to ensure the meaningful values of the prior parameter distribution (Lunn et al., 2013). Each β_i parameter must be positive (Sect. 3.2.2) so we truncated the normal distribution on each β_i except θ to ensure only positive values. For θ, we truncated the normal distribution to occur between 0 and 1 by setting the obvious limit to this parameter (see also item 2 in Sect. 3.2.2). The above choices ensure wide non-informative prior distributions whilst specifically excluding physically unrealistic values.

3.2.2 Informative prior distributions

Below we justify choices for the prior parameters on $\boldsymbol{\beta}$.

1. The quantum yield, α, represents the amount of absorbed CO_2 per quanta of absorbed light. Cannell and Thornley (1998) reported that α varies little among C_3 species and has a value from 0.09 to 0.11 and from 0.04 to 0.075 mol CO_2 (mol quanta)$^{-1}$ in saturated and ambient CO_2 conditions respectively. The typical value of α equals 0.05 mol CO_2 (mol quanta)$^{-1}$ for a C_3 species in an ambient atmosphere (Skillman, 2008; Long et al., 2006; Bonan et al., 2002). Douglas fir at Speulderbos is a C_3 species. We used this information to construct the prior distribution on α, as follows:

BGD
12, 13967–14002, 2015

- A value of α around 0.05 has the highest probability. The probability decreases as the value of α decreases or increases from 0.05 and cannot be negative. The maximum value that α can attain is 0.11.
- We assumed a normal distribution of α with mean, $\mu_\alpha = 0.05$, and variance, $\sigma_\alpha^2 = (0.015)^2$ (i.e, standard deviation, $\sigma_\alpha = 0.015$). The choice of mean ensures that the highest probability is assigned to the values around 0.05. The choice of variance ensures that 99.7 % ($\mu \pm 3\sigma_\alpha$) of α is positive and lies in the interval between 0 and 0.11. We also truncated 0.3 % of negative α values from the assumed normal distribution. In the unit of mg CO_2 (µmol quanta)$^{-1}$, the assumed normal distribution ($N(\mu_\alpha = 0.05, \sigma_\alpha = 0.015)$) is expressed as $N(0.0022, 0.00066)$ (Fig. 1a).

2. The curvature parameter θ can take values from 0, which reduces Eq. (4) to the simpler rectangular hyperbola, to 1, which describes the Blackman response of two intersecting lines (Blackman, 1905). The physiological range for θ has been observed to be between 0.5 and 0.99 (Ogren, 1993; Cannell and Thornley, 1998). A value of $\theta = 0.9$ was recommended by Thornley (2002) and at $\theta = 0.8$ by Johnson et al. (2010) and Johnson (2013). The estimate of θ, as a result of fitting the NRH model to either measured photosynthesis or NEE data was found to be in the range of 0.7 to 0.99 (Gilmanov et al., 2010, 2003). These findings for θ indicated that a higher probability should be assigned to the values around 0.8 and the probability should approach to zero below 0.5. This means that the distribution of θ can be assumed to be negatively skewed with $\Pr(\theta < 0.5)$ approaching zero and $\Pr(\theta \approx 0.8)$ at a maximum. These conditions were modelled using a beta distribution with shape parameters at 10 and 3 for θ (Fig. 1b).

3. The photosynthetic capacity at light saturation A_{max} is reached when the photosynthesis is Rubisco limited and varies among different tree species (Cannell and Thornley, 1998). We compiled the prior information on A_{max} for Douglas fir species from the literature. Values of A_{max} were mainly reported for needles,

BGD
12, 13967–14002, 2015

whereas the NRH model (Eq. 4) requires A_{max} values for the canopy. Scaling A_{max} from needle to canopy equivalents is not a trivial task as this depends on the light distribution and the vertical profile of A_{max} in the canopy. Here we analysed plateau values of photosynthesis at needle and canopy level with simulations by a model that takes this into account: the model SCOPE (van der Tol et al., 2009). These simulations (not shown) indicated that the relation between the two plateaus (canopy : needle A_{max}) increases with leaf area index (LAI) but saturates at a value of 2.8. The mean value of LAI_p at the Speulderbos site high (approximately 9 van Wijk et al., 2000; Steingrover and Jans, 1994) and therefore we could translate the reported range of A_{max} values for the Speulderbos (Mohren, 1987) of 0.26 to 0.52 mg CO_2 m^{-2} s^{-1} into values of 0.73–1.46 mg CO_2 m^{-2} s^{-1} for canopy A_{max}. van Wijk et al. (2002) reported slightly higher canopy A_{max} values of 1.86 and 1.06 mg CO_2 m^{-2} s^{-1} at the Speulderbos site. The highest and lowest value for needle A_{max} for Douglas fir (irrespective of the site) we found in the literature were 0.097 (canopy A_{max} = 0.27) and 1.01 mg CO_2 m^{-2} s^{-1} (canopy A_{max} = 2.8) respectively (Ripullone et al., 2003; Warren et al., 2003; Lewis et al., 2000). To cover this rather wide range of values, a Gamma distribution with shape and rate parameters equal to 4 and 2.5 respectively was selected to ensure higher probabilities are assigned to the values between 1 and 2.5 with decreasing probabilities down to 0 and up to 4.5 (Fig. 1c). The A_{max} values at Speulderbos are well placed in the overall distribution.

4. The parameters for temperature sensitivity k_T and Q_{10} are related as $Q_{10} = \exp(10k_T)$ (Davidson et al., 2006). Q_{10} is the factor by which respiration (Eq. 3) is multiplied when temperature increases by 10 °C. (Mahecha et al., 2010) carried out experiments across 60 FLUXNET sites to check the sensitivity of ecosystem respiration to air temperature. They suggested that Q_{10} does not differ among biomes and is confined to values around 1.4 ± 0.1 (corresponding to k_T around 0.034 ± 0.008). Hence $k_T \approx 0.034$ should have the highest probability of occur-

BGD
12, 13967–14002, 2015

rence. Q_{10} data reported in the supporting material of Mahecha et al. (2010) showed that that Q_{10} becomes less frequent as it increases or decreases from 1.4 and attains a highest value of ~ 2.72 (corresponding to $k_T = 0.1$). To model these conditions a Gamma prior distribution was chosen with shape and rate parameters equal to 4 and 120 respectively (Fig. 1d).

5. The r_0 parameter represents the ecosystem respiration at 0 °C. We adopted the following steps to define the prior distribution for r_0.

   – Mahecha et al. (2010) presented a graph of seasonal variation of ecosystem respiration at 15 °C (R_b) for 60 FLUXNET sites. We extracted the values of R_b (in g $CO_2\,m^{-2}\,day^{-1}$) from the graph for those sites that belong to evergreen needle leaf forest (ENF). We obtained the values of r_0 from R_b using the following equations:

$$r_0 = \frac{R_b}{\exp(k_T \times 15)} \tag{7}$$

   where k_T was obtained from Q_{10} as reported in point 4 above. Site specific Q_{10} value is used here. The unit of r_0 is converted into mg $CO_2\,m^{-2}\,s^{-1}$.

   – We identified values of r_0 for ENF in the range 0.013 to 0.07 mg $CO_2\,m^{-2}\,s^{-1}$. We also identified values of r_0 in the range 0.019 to 0.043 at the Loobos FLUXNET site in the Netherlands (Mahecha et al., 2010), which is close to Speulderbos. Therefore, we assumed that the most frequent values of r_0 at Speulderbos are in this range. To model these conditions we chose a Beta distribution with shape parameters at 2 and 64 (Fig. 1e).

3.3 Bayesian inference of β

We used WinBUGS software version 1.4.3 (Lunn et al., 2000) to implement the Bayesian full probability models (Eq. 5) for the inference of $\boldsymbol{\beta}$. WinBUGS is a window

BGD
12, 13967–14002, 2015

based interface of the BUGS (Bayesian Inference Using Gibbs Sampling) software. This was a joint initiative of the MRC Biostatistics Unit, Cambridge and the Imperial College School of Medicine, London (Lunn et al., 2013). WinBUGS implements MCMC methods for Bayesian inference. The major inputs of WinBUGS are: (a) the model file specifying the definition of the prior distribution of each β_i and likelihood function, (b) the number of Markov chains to create, (c) the number of iterations for MCMC to carry out for each Markov chain, (d) the burn-in period for which the MCMC runs are discarded, (e) initial values of each β_i for each Markov chain. The burn-in period is the number of samples after which the Markov chains converge to a stationary distribution. The post burn-in samples are used to perform inference on the β_i s.

We obtained the posterior distribution of each β_i for every 10-day block (total 22 blocks) in the growing season of 2009. The 10-day block was chosen because it was sufficiently long to ensure a suitably large NEE dataset *within* the 10-day block but was short enough that we could observe temporal change *between* the 10-day blocks. Temporal variation arose due to changes in canopy structure, soil moisture and ecosystem nutrient levels (Aubinet et al., 2012). The sample size within a 10-day block was limited because $\sim 30\,\%$ of the data were typically discarded as being of low quality (Foken flag 4 or higher, see Sect. 3.1).

We identified the appropriate length of the burn-in for both informative and non-informative prior distributions. We calculated the Gelman–Rubin potential scale reduction factor (PSRF) diagnostics to evaluate the convergence of the Markov chains for each β_i for the post burn-in period. A detailed explanation of PSRF and the identification of the length of the burn-in are given in the Supplement. Based on that analysis we used three Markov chains with 16 000 and 25 000 iterations for each chain for informative and non-informative prior distributions respectively. We stored the posterior samples of each β_i and τ_e for the remaining 30 000 samples (i.e., 10 000 post burn-in samples for each of three Markov chains). The BUGS code (model file for WinBUGS) is given in the Supplement.

BGD
12, 13967–14002, 2015

3.4 Posterior prediction

To perform prediction for a given PPFD_0 and T_{a_0}, m post burn-in samples of $\boldsymbol{\beta}$ and σ^2 were used as follows:

$$\mu_0^{(l)} = \frac{1}{2\theta^{(l)}} \times \left(\alpha^{(l)} \cdot \mathrm{PPFD}_0 + A_{\max}^{(l)} - \sqrt{(\alpha^{(l)} \cdot \mathrm{PPFD}_0 + A_{\max}^{(l)})^2 - 4\alpha^{(l)} \cdot A_{\max}^{(l)} \cdot \theta^{(l)} \cdot \mathrm{PPFD}_0}\right)$$

$$v_0^{(l)} = r_0^{(l)} \times \exp\left(k_{\mathrm{T}}^{(l)} T_{a_0}\right)$$

$$y_0^{(l)} \sim N(\mu_0^{(l)} - v_0^{(l)}, \sigma^{2(l)}) \quad (8)$$

where (l) is not an exponent, but indicates a specific sample. Other terms are as defined for Eq. (6). The m samples were used to build up the posterior predictive distribution. In this way posterior predictions of GPP (μ_0) and NEE (y_0) were obtained. Note that the uncertainty in the posterior predictions of GPP arose due to uncertainty in the posterior estimates of $\boldsymbol{\beta}$. Uncertainty in the posterior prediction of NEE also considered the uncertainty arising due to the residual error.

Prediction was performed for each 10-day sample for m = 30 000 samples (3 chains and 10 000 samples per chain). These were then summarized (median and 95 % credible interval) to obtain the posterior predictive inference for NEE and GPP for each 10-day block. These 95 % credible intervals show the uncertainty. We reported the number of half-hourly NEE measurements that lie inside and outside of 95 % credible intervals of the corresponding half-hourly modelled NEE distributions. In this way, we checked whether realistic credible intervals were obtained. Validation against a separate or hold-out dataset was in principle possible, but was not necessary in this study, because we did not use the NRH model to predict to blocks without data. Moreover, we did not use the posterior $\boldsymbol{\beta}$ values outside the blocks where they were fitted.

BGD
12, 13967–14002, 2015

4 Results

4.1 Performance of MCMC

We examined the trace plots of the three Markov chains for each β_i and τ_e obtained for each 10-day block for both choices of informative and non-informative prior distributions. Trace plots for one 10-day block (1 May to 10 May 2009) are shown in Fig. S3 in the Supplement. The chains were thoroughly interdigitating, indicating that the the Markov chains had mixed and converged to a stationary distribution and could be used for inference. The Gelman–Rubin PSRF was close to 1 (Table S1 in the Supplement) for each β_i and τ_e, providing further support for the convergence of the Markov chains. The post burn-in samples were used for inference for each 10-day block in the growing season of 2009.

Figure 2 shows the posterior prediction of half-hourly NEE for a 10-day block (1 May to 10 May 2009) for the choice of informative and non-informative prior distributions. The half-hourly NEE was summarized by the median and the 2.5 and 97.5 % iles (i.e., 95 % credible intervals). Out of 338 available half-hourly NEE measurements in this 10-day block, 6 % lay outside the 95 % credible intervals for both choices of prior distribution. This showed that the coverage of the 95 % credible interval was accurate. There was no substantial difference in the shape of the percentiles curve between the choices of prior distribution. This indicated that the choice of informative or non-informative priors did not influence the posterior prediction of NEE. Similar results were observed for other 10-day blocks. Over the entire 2009 growing season 94 % of the 7126 available half-hourly NEE measurements were bracketed by the 95 % credible intervals for posterior predicted NEE. The choice of informative or non-informative priors did not lead to any substantial difference in the posterior predicted median or 95 % credible intervals.

The 10-day block shown in Fig. 2 shows that the posterior predicted median of NEE was positive during the day and negative during the night. This is to be expected owing to the lack of photosynthesis at night. However, at night the 95 % credible interval spanned zero implying that, when prediction uncertainty is considered, the predicted

BGD
12, 13967–14002, 2015

NEE *might* be positive. This is not possible physically, so it is important to understand how this result was achieved and what it means. Since this is a non-linear regression-type problem the uncertainty in the prediction arises due to both the uncertainty in the estimated regression parameters, $\boldsymbol{\beta}$ and the residual uncertainty. This residual uncertainty was assumed to follow a normal distribution with zero mean and precision, τ_e, and reflects the scatter of the observations round the posterior median prediction. Following our discussion above, this correctly represents the uncertainty in prediction. A consequence of this was that that the prediction intervals were wide and the predictions were potentially positive during the night. This could potentially be addressed by introducing further constraints into the model to allow τ_e to vary temporally (e.g., Hamm et al., 2012). We leave that as a topic for future research whilst noting that our dataset is not very large and we have already fitted a complicated model.

4.2 Uncertainty in partitioned GPP at half-hourly and daily time step

Figure 3 shows the histograms of the posterior distribution of half-hourly and daily-summed GPP for Julian days 121 (1 May) and 196 (15 July) for the choice of both informative and non-informative prior distributions. These allow visualization of the uncertainty within a day and between days for late spring and mid-summer. It is clear that the predictions resulting from informative and non-informative priors were similar. For both days higher values of GPP were observed in the afternoon compared to the morning on both Julian days. This reflected the increase in GPP predictions with increasing PPFD from morning to afternoon. The assimilation of carbon was also expected to increase from the start of the growing season to the peak (summer time) of the growing season. It was clear that higher values in GPP were predicted on Julian day 196 compared to Julian day 121 for both morning and afternoon. Seasonal variation in daily GPP was also observed in the daily sum of GPP, which increased from 7–9 $\mathrm{g\,C\,m^{-2}\,d^{-1}}$ on Julian day 121 to 10.5–12.5 $\mathrm{g\,C\,m^{-2}\,d^{-1}}$ on Julian day 196. Variation in daily GPP during the 2009 growing season is shown in Fig. S4.

BGD
12, 13967–14002, 2015

4.3 Posterior distributions of β

Figure 4 and 5 show the temporal profile (mean and 95 % credible interval) for $\boldsymbol{\beta}$ for each 10-day block for informative and non-informative prior $\boldsymbol{\beta}$ distributions respectively.

A clear seasonal pattern in the posterior distribution of α and A_{max} was observed. When using non-informative priors, spikes in the 97.5 % iles for A_{max} were observed at 41, 47, and 59 $mg\,CO_2\,m^{-2}\,s^{-1}$ (Fig. 5e) for three 10-day blocks (Julian days 91–100, 281–290, and 291–300). These values are physically unrealistic (see Sect. 3.2.2). When using informative priors, the same three 10-day blocks also showed spikes in the 97.5 % iles for A_{max} (Fig. 4e); however these spikes were much smaller and were physically realistic. For other 10-day blocks, both choices of prior yielded comparable posterior distributions of A_{max} (Figs. 4e and 5f) with uncertainty less than that of the informative and non-informative prior distributions (Fig. 1c and Sect. 3.2.1). The posterior distributions of α, r_0, and k_T were similar for both choices of prior distribution. The choice of non-informative prior yielded wider credible intervals for θ compared to the choice of informative priors (Figs. 4b and 5b).

We calculated the sum of daily GPP for each of the above mentioned 10-day blocks (91–100, 281–290, and 291–300) for both choices of prior (Fig. S5). We found no significant difference in the range of GPP for each block. For example, the range of daily-summed values for 10-day block 281–290 was 26–38 $g\,C\,m^{-2}\,d^{-1}$ for both choices of prior. This indicated that the unrealistic spikes in the posterior distributions of A_{max} did not affect the prediction of GPP.

5 Discussion

5.1 Choice of informative and non-informative prior for β

In order to undertake a Bayesian analysis it is necessary to specify the prior distributions on the NRH parameters. We compared the impact of the choice of informative

BGD
12, 13967–14002, 2015

and non-informative priors on the posterior distributions of the NRH parameters and on posterior prediction of GPP and NEE. The resulting posterior distributions for NEE and GPP were similar, but for one of the parameters, notably A_{max}, non-informative priors led to unrealistic values in the posterior. Such unrealistic values were not observed when informative priors were chosen. Nevertheless, those unrealistic values did not affect the posterior predictions of GPP and NEE. This led us to evaluate the sensitivity of GPP to A_{max}. We fixed the value of the NRH parameters α, θ, r_0, and k_T at their mean and estimated the values of GPP (Eq. 2) by varying A_{max} from 0 to 100 mg CO_2 m^{-2} s^{-1}. This wide variation in A_{max} was chosen as the non-informative priors led to spikes in the value of A_{max} in the posterior (Fig. 5e).

The plot of A_{max} against GPP (Fig. 6) revealed that GPP varied strongly up to A_{max} = 5 mg CO_2 m^{-2} s^{-1}. After this value GPP saturated. The underlying reason is the fact that in light limited conditions, i.e., $A_{max} \gg \alpha \times$ PPFD, Eq. (2) reduces to $P_a = \alpha \times$ PPFD and hence P_a and thus GPP becomes independent of A_{max}. This explains why the GPP and NEE posterior predictions were not affected by the unrealistic values of A_{max} occurring in periods of low light intensities. The choice of prior distribution therefore played a minimal role in the prediction of GPP. The use of informative priors, however, constrained the estimation of the posterior distributions of the parameters.

5.2 Distributions of GPP at different time steps

We tested whether in the posterior half-hourly GPP distributions, the non-rectangular hyperbolic relationship of GPP with PPFD has been preserved. Figure 7 shows that for an example 10-day period block (Julian days 121–130), posterior GPP versus PPDF. The resulting curves shows that the non-rectangular hyperbolic relationship is indeed preserved, and GPP values initially rise and later reach a plateau with increasing PPFD. This is important since our daily GPP estimates were obtained by summing half-hourly values. Since the range of PPDF values during the day is large and the relationship between PPFD and GPP non-linear, a realistic representation of the light response

BGD
12, 13967–14002, 2015

curve of GPP is important. We note that many process-based simulators of GPP, such as such as BIOME-BGC, do not integrate instantaneous GPP over the diurnal cycle to obtain daily values, but instead estimate daily GPP from averaged input values (for example, daily average PPFD). Hence process-based simulators do not incorporate the effects of the non-linearity of the model during the diurnal cycle (Wang et al., 2014).

We conclude that the posterior predictions of half-hourly and daily GPP were reliable. We used the posterior distribution of the NRH parameters to predict half-hourly NEE and the 95 % credible intervals bracketed 94 % of the available half-hourly NEE measurements (Sect. 4.1 and Fig. 2). This indicated that our posterior predictions accurately captured the uncertainty in the measured NEE values. We used the same posterior distributions of the NRH parameters to estimate uncertainty in half-hourly GPP. Therefore, we expect that the underlying uncertainty in half-hourly GPP was also accurate.

5.3 Estimating uncertainty using the NRH model

The Bayesian approach applied to the NRH model is a solid method to quantify the model parameters and their uncertainty. The 10-day block although suited for the purpose of this study, is insufficient to incorporate the effects of more rapid changes (day to day) in soil moisture and nutrient levels in the NRH model. In principle, these rapid changes could be incorporated by daily estimation of the NRH parameters (Aubinet et al., 2012; Gilmanov et al., 2013), although this could not be achieved in this study due to the lack of continuous high quality half-hourly NEE data. The temporal variation in soil moisture and nutrient level for the study site should be investigated further. This may help to select an optimum block size where the within-block variation is limited. The availability of continuous high quality NEE data, however, may impose further constraints on the selection of an optimum block size.

This study excluded the effect of VPD as a limiting factor for the water stress at the study site by following the previously published value of VPD_{cr} (Sect. 3.1). VPD_{cr} varies between vegetation types and ecosystem (Lasslop et al., 2010). VPD_{cr} should

BGD
12, 13967–14002, 2015

be defined further for Douglas fir at the study site. Higher VPD, i.e., greater than site specific VPD_{cr}, may produce an asymmetric shape in diurnal NEE. By incorporating site specific VPD_{cr}, it is expected that overestimation and underestimation of NEE will be reduced (Fig. 2).

The implementation of the NRH model assumed that PPFD and T_a were known without error and all uncertainty was attributed to the response variables. This assumption is useful in such statistical models, but is likely to be simple in this case. There is scope to incorporate additional information about uncertainty in PPFD and T_a. This can be done by defining distribution functions for PPFD and T_a in the Bayesian probability model.

We focused in this study on the growing season in 2009. This short period was chosen to illustrate the implementation of the Bayesian approach to quantify the uncertainty in half-hourly partitioned GPP using the NRH model. The study could be extended towards multiple years thus resulting a multi-year comparison, but that is outside the scope of the current methodological focus. Also, different models have been investigated previously to partition GPP (Desai et al., 2008; Richardson et al., 2006). Any model as its own approximation of reality is a source of systematic uncertainty in itself. The scope of this study can therefore be further widen by addressing multiple established ways of partitioning GPP and thus analysing systematic uncertainty associated with these.

6 Conclusions

Quantifying uncertainty estimates as empirical distributions in half-hourly gross primary production (GPP) was possible in a Bayesian framework using the non-rectangular hyperbola (NRH) model. These uncertainty estimates were provided at daily time steps. The approach could be extended to include the uncertainty in meteorological forcing, in particular photosynthetic photon flux density and air temperature. The distributions in half-hourly GPP can be used further to obtain distributions at any desired time steps,

BGD
12, 13967–14002, 2015

such as 8 days and monthly. The uncertainty in GPP estimated in this study can be used to quantify the propagated uncertainty in the validation of satellite GPP products such as MODIS 17 or process-based simulators such as BIOME-BGC.

We also reported the uncertainty in half-hourly modelled net ecosystem exchange (NEE). The uncertainty in NEE brackets most of the NEE measurements. It could further be investigated how much of the uncertainty in NEE measurements is due to random and systematic errors using the same Bayesian framework.

The estimates of the NRH model parameters were obtained for 10-day blocks. The values of the posterior parameters and their variation over time could provide further understanding of how the forest responds to factors not included in the model, such as soil moisture, nutrition or tree age.

The study further concluded that the choice of informative and non-informative prior distributions of the NRH model parameters led to similar posterior distributions for both GPP and NEE. Obtaining informative priors is time consuming as the values of each parameter are not explicitly mentioned in the literature. Informative priors also require to gather information on species or site specific values of photosynthetic capacity at light saturation (A_{max}) and ecosystem respiration at reference temperature (r_0) parameter. As an alternative, non-informative priors can be obtained with proper constraints using minimum information on the NRH parameters such as the positivity of A_{max}. Therefore, non-informative priors should be considered, which can be used for any species type irrespective of study sites. These findings are valuable to conduct uncertainty analysis across a larger sample of sites with different GPP characteristics, e.g., by obtaining NEE and other meteorological data from the FLUXNET data base. The downside of non-informative prior is the production of spikes in the posterior of A_{max} for some days in this study. Therefore, if such values are of interest in a particular study, e.g., photosynthesis nitrogen use efficiency that relies on the ratio of A_{max} and leaf nitrogen, then informative prior should be considered.

BGD
12, 13967–14002, 2015

The Supplement related to this article is available online at doi:10.5194/bgd-12-13967-2015-supplement.

Acknowledgements. The authors thankfully acknowledge the support of the Erasmus Mundus mobility grant and the University of Twente for funding this research.

References

Aubinet, M., Vesala, T., and Papale, D.: Eddy Covariance: A Practical Guide to Measurement and Data Analysis, 1st edn., Springer, Dordrecht, The Netherlands, 2012. 13969, 13970, 13980, 13986

Baldocchi, D. D.: Assessing the eddy covariance technique for evaluating carbon dioxide exchange rates of ecosystems: past, present and future, Glob. Change Biol., 9, 479–492, 2003. 13969

Blackman, F. F.: Optima and limiting factors, Ann. Bot., 19, 281–296, 1905. 13977

Bonan, G. B., Levis, S., Kergoat, L., and Oleson, K. W.: Landscapes as patches of plant functional types: an integrating concept for climate and ecosystem models, Global Biogeochem. Cy., 16, 5-1–5-23, 2002. 13976

Cannell, M. G. R. and Thornley, J. H. M.: Temperature and CO_2 responses of leaf and canopy photosynthesis: a clarification using the non-rectangular hyperbola model of photosynthesis, Ann. Bot., 82, 883–892, 1998. 13976, 13977

Davidson, E. A., Janssens, I. A., and Luo, Y.: On the variability of respiration in terrestrial ecosystems: moving beyond Q10, Glob. Change Biol., 12, 154–164, 2006. 13978

Desai, A. R., Richardson, A. D., Moffat, A. M., Kattge, J., Hollinger, D. Y., Barr, A., Falge, E., Noormets, A., Papale, D., Reichstein, M., and Stauch, V. J.: Cross-site evaluation of eddy covariance GPP and RE decomposition techniques, Agric. Forest Meteorol., 148, 821–838, 2008. 13987

Du, Z., Nie, Y., He, Y., Yu, G., Wang, H., and Zhou, X.: Complementarity of flux-and biometric-based data to constrain parameters in a terrestrial carbon model, Tellus B, 67, doi:10.3402/tellusb.v67.24102, 2015. 13971

Foken, T., Göockede, M., Mauder, M., Mahrt, L., Amiro, B., and Munger, W.: Post-field data quality control, in: Handbook of Micrometeorology, edited by Lee, X., Massman, W., and

BGD
12, 13967–14002, 2015

Law, B., vol. 29 of Atmospheric and Oceanographic Sciences Library, Chap. 9, Springer, Dordrecht, The Netherlands, 181–208, 2005. 13974

Gelman, A., Carlin, J. B., Stern, H. S., Dunson, D. B., Vehtari, A., and Rubin, D. B.: Bayesian Data Analysis, CRC Press, Boca Raton, 2013. 13971, 13973

Gilmanov, T. G., Verma, S. B., Sims, P. L., Meyers, T. P., Bradford, J. A., Burba, G. G., and Suyker, A. E.: Gross primary production and light response parameters of four Southern Plains ecosystems estimated using long-term CO_2-flux tower measurements, Global Biogeochem. Cy., 17, 2, doi:10.1029/2002GB002023, 2003. 13970, 13972, 13977

Gilmanov, T. G., Aires, L., Barcza, Z., Baron, V. S., Belelli, L., Beringer, J., Billesbach, D., Bonal, D., Bradford, J., Ceschia, E., Cook, D., Corradi, C., Frank, A., Gianelle, D., Gimeno, C., Gruenwald, T., Guo, H., Hanan, N., Haszpra, L., Heilman, J., Jacobs, A., Jones, M. B., Johnson, D. A., Kiely, G., Li, S., Magliulo, V., Moors, E., Nagy, Z., Nasyrov, M., Owensby, C., Pinter, K., Pio, C., Reichstein, M., Sanz, M. J., Scott, R., Soussana, J. F., Stoy, P. C., Svejcar, T., Tuba, Z., and Zhou, G.: Productivity, respiration, and light-response parameters of world grassland and agroecosystems derived from flux-tower measurements, Rangeland Ecol. Manag., 63, 16–39, 2010. 13977

Gilmanov, T. G., Wylie, B. K., Tieszen, L. L., Meyers, T. P., Baron, V. S., Bernacchi, C. J., Billesbach, D. P., Burba, G. G., Fischer, M. L., Glenn, A. J., Hanan, N. P., Hatfield, J. L., Heuer, M. W., Hollinger, S. E., Howard, D. M., Matamala, R., Prueger, J. H., Tenuta, M., and Young, D. G.: CO_2 uptake and ecophysiological parameters of the grain crops of midcontinent North America: estimates from flux tower measurements, Agric. Ecosyst. Environ., 164, 162–175, 2013. 13970, 13972, 13974, 13986

Hagen, S. C., Braswell, B. H., Linder, E., Frolking, S., Richardson, A. D., and Hollinger, D. Y.: Statistical uncertainty of eddy flux-based estimates of gross ecosystem carbon exchange at Howland Forest, Maine, J. Geophys. Res.-Atmos., 111, D08S03, doi:10.1029/2005JD006154, 2006. 13970

Hamm, N. A. S., Atkinson, P. M., and Milton, E. J.: A per-pixel, non-stationary mixed model for empirical line atmospheric correction in remote sensing, Remote Sensing Environ., 124, 666–678, 2012. 13983

Johnson, I. R.: PlantMod: exploring the physiology of plant canopies, IMJ Software, Melbourne, Australia, 2013. 13977

BGD
12, 13967–14002, 2015

Johnson, I. R., Thornley, J. H. M., Frantz, J. M., and Bugbee, B.: A model of canopy photosynthesis incorporating protein distribution through the canopy and its acclimation to light, temperature and CO_2, Ann. Bot., 106, 735–749, 2010. 13977

Körner, C.: Leaf Diffusive Conductances in the Major Vegetation Types of the Globe, in: Ecophysiology of Photosynthesis, edited by: Schulze, E. D. and Caldwell, M. M., vol. 100 of Springer Study Edition, Chap. 22, Springer-Verlag, New York, 463–490, 1995. 13975

Lasslop, G., Reichstein, M., Papale, D., Richardson, A. D., Arneth, A., Barr, A., Stoy, P., and Wohlfahrt, G.: Separation of net ecosystem exchange into assimilation and respiration using a light response curve approach: critical issues and global evaluation, Glob. Change Biol., 16, 187–208, 2010. 13969, 13970, 13975, 13986

Lewis, J. D., McKane, R. B., Tingey, D. T., and Beedlow, P. A.: Vertical gradients in photosynthetic light response within an old-growth Douglas-fir and western hemlock canopy, Tree Physiol., 20, 447–456, 2000. 13978

Li, X., Liang, S., Yu, G., Yuan, W., Cheng, X., Xia, J., Zhao, T., Feng, J., Ma, Z., Ma, M., Liu, S., Chen, J., Shao, C., Li, S., Zhang, X., Zhang, Z., Chen, S., Ohta, T., Varlagin, A., Miyata, A., Takagi, K., Saiqusa, N., and Kato, T.: Estimation of gross primary production over the terrestrial ecosystems in China, Ecol. Model., 261/262, 80–92, 2013. 13969

Long, S. P., Zhu, X.-G., Naidu, S. L., and Ort, D. R.: Can improvement in photosynthesis increase crop yields?, Plant Cell Environ., 29, 315–330, 2006. 13976

Lunn, D., Thomas, A., Best, N., and Spiegelhalter, D.: WinBUGS – a Bayesian modelling framework: Concepts, structure, and extensibility, Stat. Comput., 10, 325–337, 2000. 13979

Lunn, D., Jackson, C., Best, N., Thomas, A., and Spiegelhalter, D.: The BUGS Book – A Practical Introduction to Bayesian Analysis, CRC Press, Boca Raton, 2013. 13975, 13976, 13980

Mahecha, M. D., Reichstein, M., Carvalhais, N., Lasslop, G., Lange, H., Seneviratne, S. I., Vargas, R., Ammann, C., Arain, M. A., Cescatti, A., Janssens, I. A., Migliavacca, M., Montagnani, L., and Richardson, A. D.: Global convergence in the temperature sensitivity of respiration at ecosystem level, Science, 329, 838–840, 2010. 13978, 13979

Minet, J., Laloy, E., Tychon, B., and François, L.: Bayesian inversions of a dynamic vegetation model at four European grassland sites, Biogeosciences, 12, 2809–2829, doi:10.5194/bg-12-2809-2015, 2015. 13971

Mohren, G. M. J.: Simulation of forest growth, applied to Douglas fir stands in the Netherlands, Ph.D. thesis, Wageningen Agriculture university, The Netherlands, 1987. 13978

BGD
12, 13967–14002, 2015

Monteith, J. L. and Unsworth, M. H.: Principles of Environmental Physics, Edward Arnold, Sevenoaks, UK, 2nd edn., 1990. 13975
Oakley, J. E. and O'Hagan, A.: Uncertainty in prior elicitations: a nonparametric approach, Biometrika, 94, 427–441, 2007. 13973
Ogren, E.: Convexity of the photosynthetic light-response curve in relation to intensity and direction of light during growth, Plant Physiol., 101, 1013–1019, 1993. 13977
Raj, R., Hamm, N. A. S., van der Tol, C., and Stein, A.: Variance-based sensitivity analysis of BIOME-BGC for gross and net primary production, Ecol. Model., 292, 26–36, 2014. 13973
Reichstein, M., Falge, E., Baldocchi, D., Papale, D., Aubinet, M., Berbigier, P., Bernhofer, C., Buchmann, N., Gilmanov, T., Granier, A., Grünwald, T., Havránková, K., Ilvesniemi, H., Janous, D., Knohl, A., Laurila, T., Lohila, A., Loustau, D., Matteucci, G., Meyers, T., Miglietta, F., Ourcival, J.-M., Pumpanen, J., Rambal, S., Rotenberg, E., Sanz, M., Tenhunen, J., Seufert, G., Vaccari, F., Vesala, T., Yakir, D., and Valentini, R.: On the separation of net ecosystem exchange into assimilation and ecosystem respiration: review and improved algorithm, Glob. Change Biol., 11, 1424–1439, 2005. 13969
Ricciuto, D. M., Davis, K. J., and Keller, K.: A Bayesian calibration of a simple carbon cycle model: The role of observations in estimating and reducing uncertainty, Global Biogeochem. Cy., 22, 2, doi:10.1029/2006GB002908, 2008. 13971
Richardson, A. D. and Hollinger, D. Y.: Statistical modeling of ecosystem respiration using eddy covariance data: Maximum likelihood parameter estimation, and Monte Carlo simulation of model and parameter uncertainty, applied to three simple models, Agric. Forest Meteorol., 131, 191–208, 2005. 13970
Richardson, A. D., Braswell, B. H., Hollinger, D. Y., Burman, P., Davidson, E. A., Evans, R. S., Flanagan, L. B., Munger, J. W., Savage, K., Urbanski, S. P., and Wofsy, S. C.: Comparing simple respiration models for eddy flux and dynamic chamber data, Agric. Forest Meteorol., 141, 219–234, 2006. 13969, 13987
Ripullone, F., Grassi, G., Lauteri, M., and Borghetti, M.: Photosynthesis–nitrogen relationships: interpretation of different patterns between *Pseudotsuga menziesii* and *Populus x euroamericana* in a mini-stand experiment, Tree Physiol., 23, 137–144, 2003. 13978
Ruimy, A., Jarvis, P., Baldocchi, D., and Saugier, B.: CO_2 fluxes over plant canopies and solar radiation: a review, Adv. Ecol. Res., 26, 1–68, 1995. 13970

BGD
12, 13967–14002, 2015

Running, S. W., Nemani, R. R., Heinsch, F. A., Zhao, M., Reeves, M., and Hashimoto, H.: A continuous satellite-derived measure of global terrestrial primary production, BioScience, 54, 547–560, 2004. 13969

Skillman, J. B.: Quantum yield variation across the three pathways of photosynthesis: not yet out of the dark, J. Exp. Bot., 59, 1647–1661, 2008. 13976

Steingrover, E. G. and Jans, W. W. P.: Physiology of forest-grown Douglas fir trees: Effect of air pollution and drought, Tech. Rep. 94/3, IBN DLO, Institute for Forestry and Nature Research, Wageningen, the Netherlands, 1994. 13974, 13978

Stoy, P. C., Katul, G. G., Siqueira, M. B. S., Juang, J.-Y., Novick, K. A., Uebelherr, J. M., and Oren, R.: An evaluation of models for partitioning eddy covariance-measured net ecosystem exchange into photosynthesis and respiration, Agric. Forest Meteorol., 141, 2–18, 2006. 13969

Su, Z., Timmermans, W. J., van der Tol, C., Dost, R., Bianchi, R., Gómez, J. A., House, A., Hajnsek, I., Menenti, M., Magliulo, V., Esposito, M., Haarbrink, R., Bosveld, F., Rothe, R., Baltink, H. K., Vekerdy, Z., Sobrino, J. A., Timmermans, J., van Laake, P., Salama, S., van der Kwast, H., Claassen, E., Stolk, A., Jia, L., Moors, E., Hartogensis, O., and Gillespie, A.: EAGLE 2006 – Multi-purpose, multi-angle and multi-sensor in-situ and airborne campaigns over grassland and forest, Hydrol. Earth Syst. Sci., 13, 833–845, doi:10.5194/hess-13-833-2009, 2009. 13974

Thornley, J. H. M.: Instantaneous canopy photosynthesis: analytical expressions for sun and shade leaves based on exponential light decay down the canopy and an acclimated non-rectangular hyperbola for leaf photosynthesis, Ann. Bot., 89, 451–458, 2002. 13977

Thornley, J. H. M. and Johnson, I. R.: Plant and crop modelling, in: A Mathematical approach to Plant and Crop Physiology, The Blackburn Press, Caldwell, New Jersey, 2000. 13972

Thornton, P. E.: Description of a numerical simulation model for predicting the dynamics of energy, water, carbon, and nitrogen in a terrestrial ecosystem, Ph.D. thesis, University of Montana, Missoula, 1998. 13969

van der Tol, C., Verhoef, W., Timmermans, J., Verhoef, A., and Su, Z.: An integrated model of soil-canopy spectral radiances, photosynthesis, fluorescence, temperature and energy balance, Biogeosciences, 6, 3109–3129, doi:10.5194/bg-6-3109-2009, 2009. 13978

van Wijk, M. T., Dekker, S. C., Bouten, W., Bosveld, F. C., Kohsiek, W., Kramer, K., and Mohren, G. M. J.: Modeling daily gas exchange of a Douglas-fir forest: comparison of three stomatal

BGD
12, 13967–14002, 2015

conductance models with and without a soil water stress function, Tree Physiol., 20, 115–122, 2000. 13978

van Wijk, M. T., Dekker, S. C., Bouten, W., Kohsiek, W., and Mohren, G. M. J.: Simulation of carbon and water budgets of a Douglas-fir forest, Forest Ecology and Management, 145, 229–241, 2001. 13974

van Wijk, M. T., Bouten, W., and Verstraten, J. M.: Comparison of different modelling strategies for simulating gas exchange of a Douglas-fir forest, Ecol. Model., 158, 63–81, 2002. 13978

Wang, F., Gonsamo, A., Chen, J., Black, T. A., and Zhou, B.: Instantaneous-to-daily GPP upscaling schemes based on a coupled photosynthesis-stomatal conductance model: correcting the overestimation of GPP by directly using daily average meteorological inputs, Oecologia, 176, 703–714, 2014. 13986

Wang, H., Jia, G., Fu, C., Feng, J., Zhao, T., and Ma, Z.: Deriving maximal light use efficiency from coordinated flux measurements and satellite data for regional gross primary production modeling, Remote Sensing Environ., 114, 2248–2258, 2010. 13969

Warren, C. R., Ethier, G. J., Livingston, N. J., Grant, N. J., Turpin, D. H., Harrison, D. L., and Black, T. A.: Transfer conductance in second growth Douglas-fir (*Pseudotsuga menziesii* (Mirb.)Franco) canopies, Plant Cell Environ., 26, 1215–1227, 2003. 13978

BGD
12, 13967–14002, 2015

Table 1. List of symbols with unit.

NEE, **y**	net ecosystem exchange	mg CO_2 m^{-2} s^{-1}
P_a	gross CO_2 assimilation	mg CO_2 m^{-2} s^{-1}
GPP	gross primary production	mg C m^{-2} s^{-1}; g C m^{-2} s^{-1}
R_{eco}	ecosystem respiration	mg CO_2 m^{-2} s^{-1}
PPFD	photosynthetic photon flux density	µmol quanta m^{-2} s^{-1}
T_a	air temperature	°C
α	quantum yield	mg CO_2 (µmol quanta)$^{-1}$
θ	degree of curvature of light response curve	unitless
A_{max}	photosynthetic capacity at light saturation	mg CO_2 m^{-2} s^{-1}
k_T	temperature sensitive parameter	(°C)$^{-1}$
r_0	ecosystem respiration at reference temperature T_a = 0 °C	mg CO_2 m^{-2} s^{-1}
τ_e	precision of the normal distribution of the likelihood	
$\boldsymbol{\beta}$	(θ, α, A_{max}, r_0, k_T)	
R_b	ecosystem respiration at reference temperature T_a = 15 °C	g CO_2 m^{-2} s^{-1}
Q_{10}	multiplication factor to respiration with 10 °C increase in T_a	
RH	relative humidity	%
VPD	vapor pressure deficit	kPa
VPD_{cr}	critical value of vapor pressure deficit	kPa
ϕ	vapor pressure deficit response function	
σ_{VPD}	curvature parameter for ϕ	kPa

BGD
12, 13967–14002, 2015

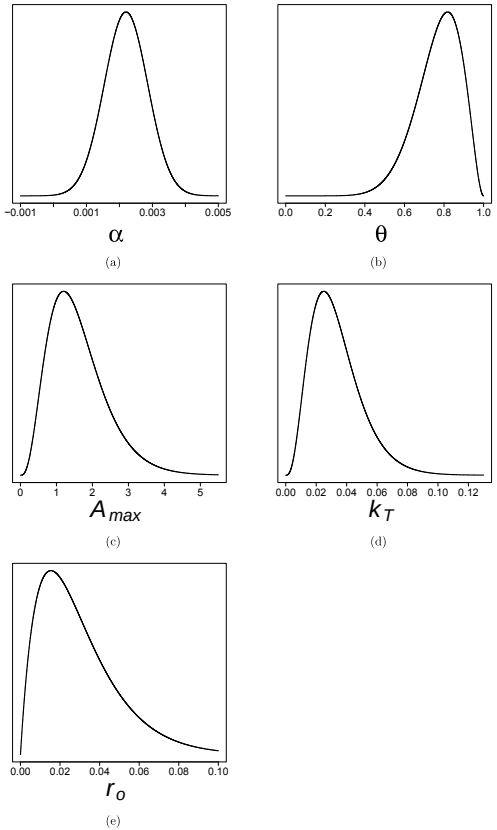

Figure 1. Informative prior distribution of the NRH model parameters: **(a)** $\alpha \sim N(\mu_\alpha = 0.0022, \sigma_\alpha = 0.00066)$, **(b)** $\theta \sim \text{Beta}(\text{shape1} = 10, \text{shape2} = 3)$, **(c)** $A_{\text{max}} \sim \text{Gamma}(\text{shape} = 4, \text{rate} = 2.5)$, **(d)** $k_{\text{T}} \sim \text{Gamma}(\text{shape} = 4, \text{rate} = 120)$, **(e)** $r_0 \sim \text{Beta}(\text{shape1} = 2, \text{shape2} = 64)$. Information about the NRH parameters is given in Table 1.

BGD
12, 13967–14002, 2015

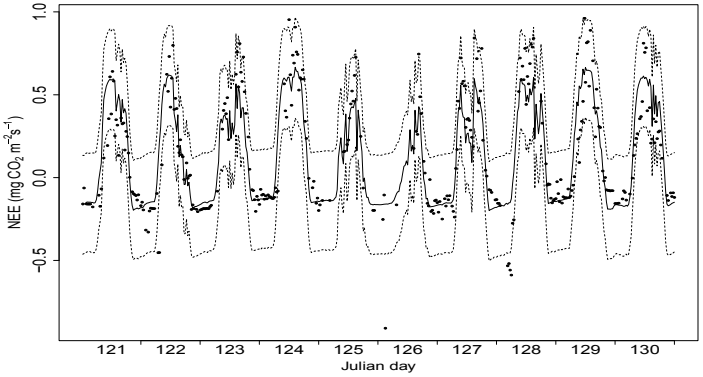

(a)

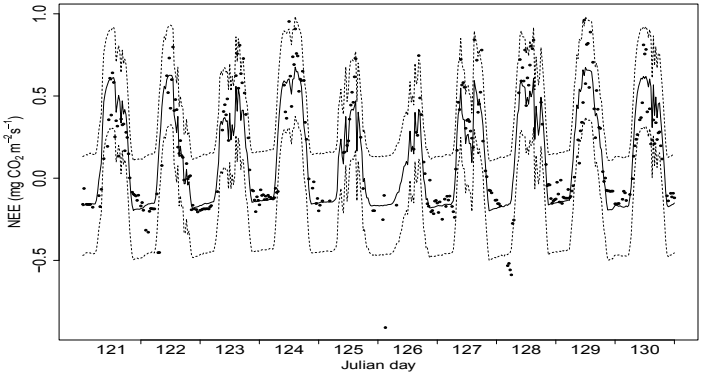

(b)

Figure 2. Median (solid lines) and 95 % credible intervals (dashed lines) of the posterior distribution of NEE together with half-hourly NEE measurements (solid points) for a 10-day block (1 May to 10 May 2009, Julian days 121 to 130): **(a)** when using informative prior distributions, **(b)** when using non-informative prior distributions.

BGD
12, 13967–14002, 2015

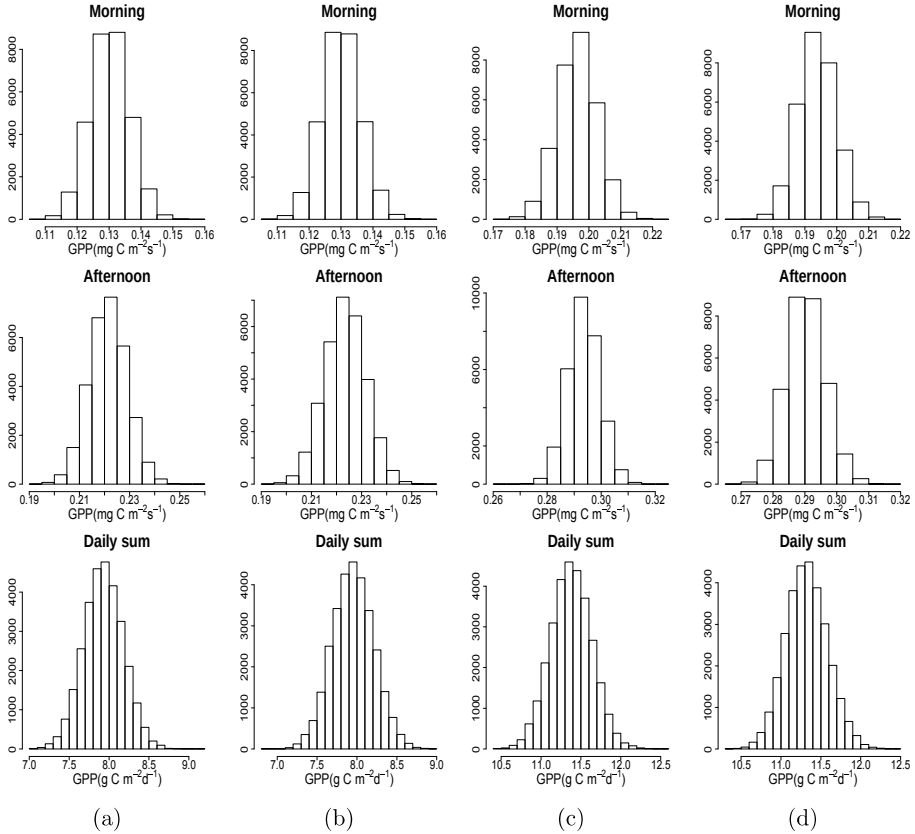

Figure 3. Histograms of half hourly GPP (Morning and afternoon) and daily sum of GPP when using: **(a)** informative priors on Julian day 121 (1 May 2009), **(b)** non-informative priors on Julian day 121, **(c)** informative priors on Julian day 196 (15 July 2009), **(d)** non-informative priors on Julian day 196. The morning and afternoon time belong to half-hour 8:00 CET to 8:30 CET and 13:00 CET to 13:30 CET respectively. The *y* axis is frequency; CET is Central European Time.

BGD
12, 13967–14002, 2015

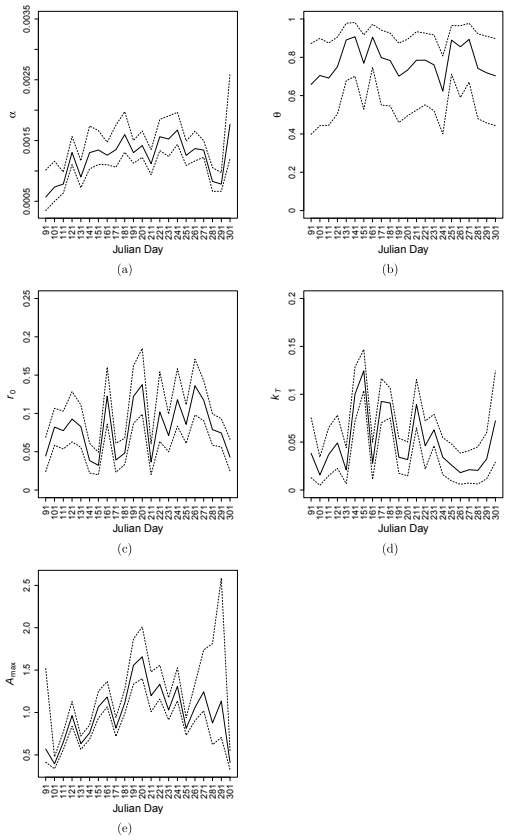

Figure 4. Median (solid lines) and 95 % credible intervals (dashed lines) of the posterior distributions of the NRH parameters when using informative prior distributions for each 10-day block during the growing season in 2009. The *x* axis is the first Julian day of each 10-day block. The *y* axis represents NRH parameter. Information about the NRH parameters is given in Table 1.

BGD
12, 13967–14002, 2015

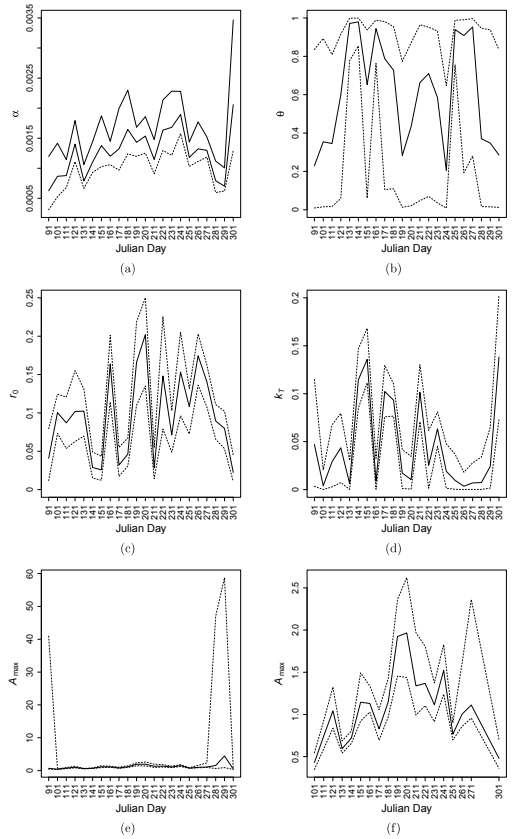

Figure 5. As Fig. 4 when using non-informative prior distributions. To help visualization of A_{max} we have added a subfigure **(f)** with the spikes removed (i.e., without the blocks of Julian days 91–100, 281–290, and 291–300).

BGD
12, 13967–14002, 2015

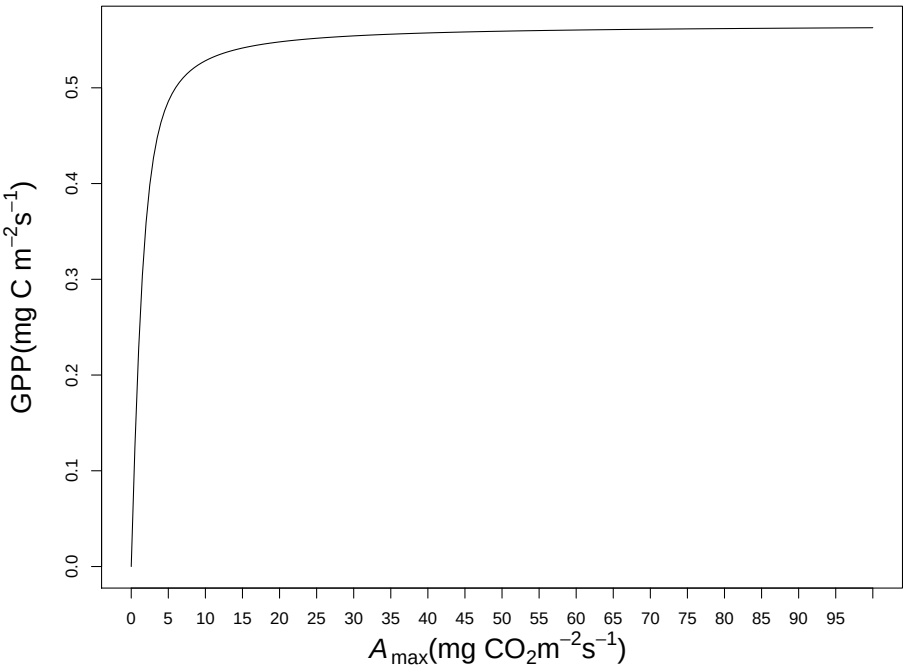

Figure 6. Variation of gross primary production (GPP) with the variation of photosynthetic capacity (A_{max}) from 0 to 100 mg CO_2 m^{-2} s^{-1}. The values of quantum yield (α), degree of curvature (θ), ecosystem respiration at reference temperature (r_0), and temperature sensitive paramete (k_T) are fixed at 0.7, 0.0022, 0.1, 0.07 respectively. Air temperature (T_a) and photosynthetic photon flux density (PPFD) are fixed at 10 °C and 900 µmol quanta m^{-2} s^{-1}.

BGD
12, 13967–14002, 2015

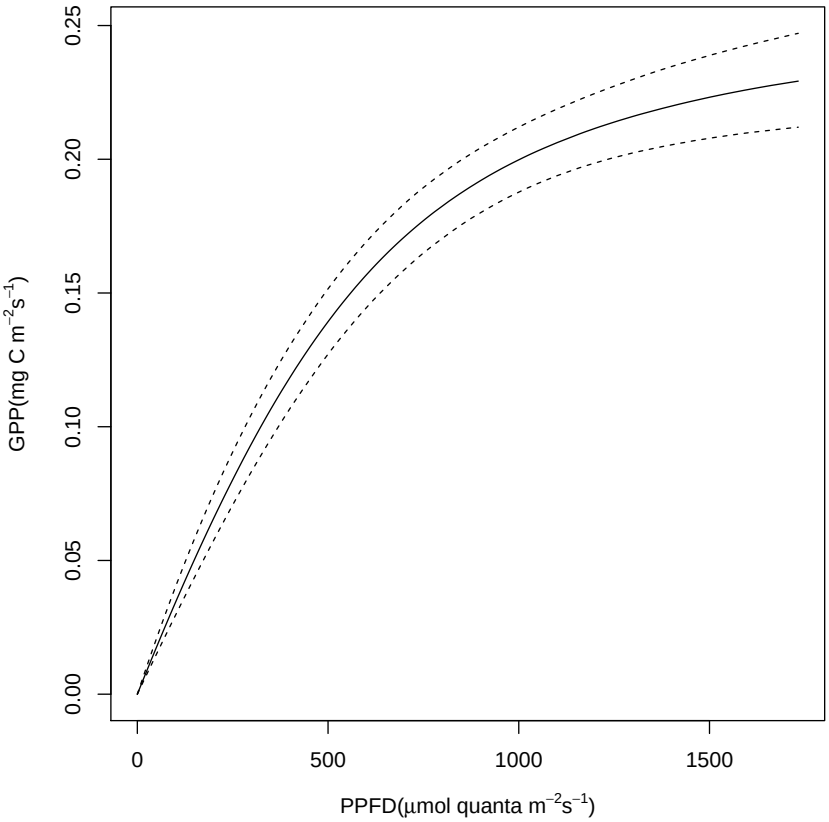

Figure 7. Median (solid line) and 95 % credible intervals (dashed lines) of half-hourly gross primary production (GPP) with photosynthetic photon flux density (PPFD) for a 10-day block (1 May to 10 May 2009, Julian days 121 to 130) for the choice of informative prior distributions.

BGD
12, 13967–14002, 2015